PHYSICAL REVIEW B **81**, 180102(R) (2010)

Direct observation of orbital ordering in the spinel oxide $FeCr_2O_4$ through electrostatic potential using convergent-beam electron diffraction

K. Tsuda,* D. Morikawa, Y. Watanabe, S. Ohtani, and T. Arima
Institute of Multidisciplinary Research for Advanced Materials, Tohoku University, 2-1-1, Katahira, Aoba-ku, Sendai 980-8577, Japan
(Received 6 February 2010; revised manuscript received 2 May 2010; published 24 May 2010)

A nanoscale structure analysis method using convergent-beam electron diffraction (CBED) has been applied to an orbital-ordered state of $Fe^{2+}3d$ electrons in a spinel oxide $FeCr_2O_4$. The atom positions, atomic displacement parameters, electrostatic potential, and electron density have been determined using CBED intensity data alone. A ferro-type ordered state of the $3z^2-r^2$ orbitals at the tetrahedrally coordinated Fe atoms has been successfully observed through the electrostatic potential obtained in the present analysis.

DOI: 10.1103/PhysRevB.81.180102 PACS number(s): 77.84.Bw, 61.05.jm, 71.20.Ps

The orbital degrees of freedom of $3d$ electrons are now recognized as hidden but very important parameters that significantly affect physical properties of strongly correlated electron systems. Various types of electron orbital ordering are caused by strong coupling with ordering of other degrees of freedom, lattice, charge, and spin (e.g., Ref. 1). A number of experimental techniques have been proposed to observe orbital-ordering states, such as polarized neutron diffraction,[2,3] resonance x-ray scattering,[4,5] charge-density analysis using synchrotron powder x-ray diffraction and maximum entropy method,[6,7] soft x-ray diffraction,[8] magnetic x-ray diffraction,[9] nuclear magnetic resonance,[10] and magnetic Compton scattering.[11] These techniques, however, do not have enough spatial resolution, especially for examining local spatial fluctuations in orbital ordering. Here, we propose a method using convergent-beam electron diffraction (CBED) to observe orbital-ordered states; the method has nanometer-scale spatial resolution.

CBED patterns can be obtained from specimen areas that are a few nanometers in diameter by using a conically converged electron beam. Structural parameters can be determined by comparing two-dimensional intensity data of CBED patterns and multiple-scattering (dynamical diffraction) calculations. Refinements of low-order structure factors, which are essential for obtaining information on valence-electron distributions, have been reported by many researchers using CBED.[12–23] Zuo *et al.*[18] reconstructed the electron-density distribution of $3d$ electrons in Cu_2O with the combined use of low-order structure factors determined by CBED and other high-order structure factors obtained from x-ray diffraction. Tsuda and Tanaka succeeded in developing a method for refining atom positions and atomic displacement parameters (Debye-Waller factors) as well as low-order structure factors using CBED intensity data alone.[17,20] The electrostatic potential distribution in a unit cell can be reconstructed from the low-order structure factors refined and the other high-order structure factors calculated with the atom positions and atomic displacement parameters.[20,23] The method of Tsuda and Tanaka enables the nanometer-scale structure analysis.

The method of Tsuda and Tanaka is applied to a spinel oxide $FeCr_2O_4$ in the present analysis. $FeCr_2O_4$ has a normal spinel structure of AB_2O_4 at room temperature. The tetrahedrally coordinated A site is occupied by an Fe^{2+} ion, which is in the high-spin $e^3t_2^3$ configuration. Thus, an electron with the minority spin in the e orbitals has an orbital degree of freedom. In contrast, the octahedrally coordinated B site is occupied by the Cr^{3+} ion, which takes the t_{2g}^3 configuration without orbital degree of freedom.[24] Thus, an orbital-ordered state of the $3d$ electrons at Fe atoms is expected in relation to a cooperative Jahn-Teller distortion. $FeCr_2O_4$ has been reported to undergo a structural phase transformation from the room-temperature cubic phase to a tetragonal phase at around 135 K.[25,26] The incident-beam directions and reflection indices are hereafter given with respect to the tetragonal system.

$FeCr_2O_4$ single crystals were grown by chemical vapor transport.[26] Thin-foil specimens for transmission electron microscopy (TEM) and CBED experiments were prepared by crushing the single crystals. Energy-filtered CBED patterns of the low-temperature phase were obtained at a specimen temperature of 90 K using an energy-filter transmission electron microscope (JEM-2010FEF) equipped with a liquid-nitrogen specimen cooling holder at an accelerating voltage of 100 kV. The microscope enables us to take energy-filtered CBED patterns up to high-scattering angles, including higher-order Laue zone (HOLZ) reflections. The intensities of the CBED patterns were recorded on imaging plates with a dynamic range of 10^6.

Figure 1(a) shows a dark-field TEM image of $FeCr_2O_4$ taken at 90 K near the [110] incidence. Stripes of 90° domains are clearly seen, which are a few tens to a few hundreds of nanometer wide. CBED patterns were obtained from single-domain areas that are a few nanometer in diameter, as indicated by a white dot in Fig. 1(a). Figure 1(b) shows energy-filtered CBED patterns taken at 90 K with the [110] incidence. The pattern contains zeroth-order Laue zone reflections at its center and HOLZ reflections appearing as a ring in the outer part, clearly showing $2mm$ symmetry. Figures 1(c) and 1(d) show energy-filtered CBED patterns taken at 90 K with the incidences of [100] and [210], showing $2mm$ and m symmetries, respectively.

Before the quantitative analysis, the space group and lattice parameters of the low-temperature phase were examined. From the symmetries of the CBED patterns of Figs. 1(b)–1(d), the point group was determined to be $4/mmm$. The lattice type was determined to be I because no hkl ($h+k+l=2n+1$, n: integer) reflections were observed. Dynami-

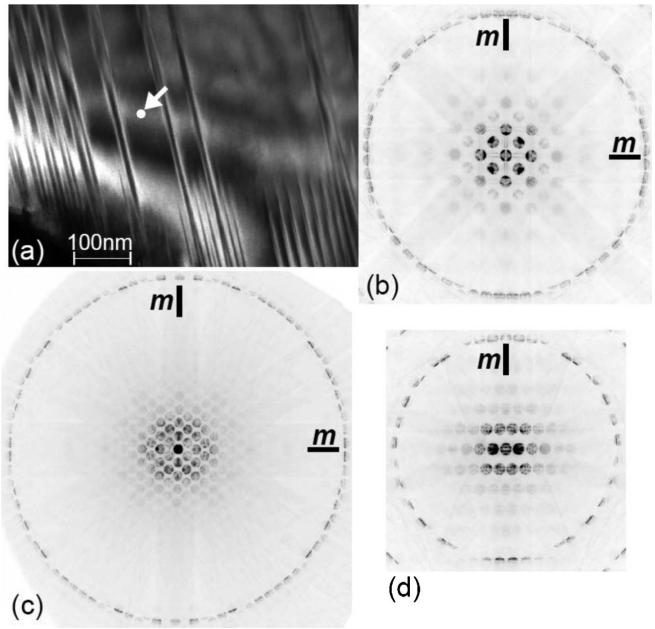

FIG. 1. (a) Dark-field TEM image of $FeCr_2O_4$ at 90 K near [110]. Energy-filtered CBED patterns taken at 90 K with (b) [110], (c) [100], and (d) [210] incidences.

cal extinctions were found in the 002 and $\bar{1}10$ reflections of the [110] pattern but not in the 1 0 $\bar{2}5$ HOLZ reflection of the [100] pattern. By referring to a table of dynamical extinction rules,[27] the space group of the low-temperature phase was uniquely determined to be $I4_1/amd$. The Wyckoff positions of atoms in the low-temperature phase with space group $I4_1/amd$ are Fe 4*a* (0, 3/4, 1/8), Cr 8*d* (0, 0, 1/2), and O 16*h* $(0,y,z)$. The lattice parameters were measured from the positions of the HOLZ lines in the CBED patterns. The determined values were $a=5.93(2)$ Å and $c=8.26(3)$ Å. These values are slightly different from those of previous reports,[25,26,28] and the ratio $c/a=0.985$ is closer to unity than the reported values. This could be due to an increase in specimen temperature by a few tens of degrees (K) caused by electron-beam illumination.

The quantitative analysis of the experimental CBED intensity data was performed according to the procedure developed by Tsuda and Tanaka.[17,20] The two-dimensional intensity data of CBED disks were extracted from the CBED patterns of Figs. 1(b)–1(d) and compared with dynamical

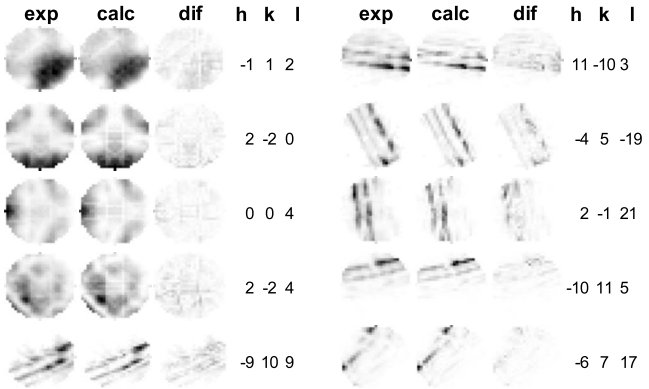

FIG. 2. Part of final result of fitting for [110] CBED pattern.

diffraction calculations. The total number of the reflection disks used for the fitting were 68, 90, and 48 for the [110], [100], and [210] data, respectively. The atom positions, atomic displacement parameters, and low-order structure factors with reciprocal vectors of $g<0.6$ Å^{-1} were refined together with experimental parameters, such as scale factors and specimen thicknesses and geometrical parameters for adjusting the positions of the CBED disks, based on a nonlinear least-squares fitting. Refinements of the parameters were conducted using the software MBFIT developed by Tsuda and Tanaka.[17,20,22,23] The reflections with excitation errors $s_g<1.0$ Å^{-1} were selected for the dynamical calculations, and those with $0.5<s_g<1.0$ Å^{-1} were treated by a perturbation (the generalized Bethe potential method[29]). A similar analysis was also applied to the room-temperature phase with the space group of $Fd\bar{3}m$ for comparison.

Figure 2 shows part of the final result of the fitting for the [110] CBED pattern of Fig. 1(b). The patterns in the left, center, and right columns show the experimental, calculated, and difference patterns of the CBED disks, respectively. The calculated patterns are in good agreement with the experimental ones. The goodness-of-fit value was 2.4. The refined values of the atom positions, anisotropic atomic displacement parameters, and low-order structure factors are shown in Table I. The specimen thicknesses determined were 922 Å, 1289 Å, and 1257 Å for the [110], [100], and [210] patterns, respectively.

Figure 3(a) shows the ORTEP diagram of the refined crystal structure of the low-temperature phase; the atomic displacement parameters are displayed as thermal ellipsoids.

TABLE I. Refined values of atom positions, anisotropic atomic displacement parameters (Å^2), and low-order structure factors (Å); numbers in parentheses denote the standard deviation of the last digit.

y(O)	0.0268(3)	U_{11}(O)	0.0055(7)	F_{013}	24.47(8)
z(O)	0.2594(1)	U_{22}(O)	0.0034(2)	F_{022}	8.48(8)
U_{11}(Fe)	0.00463(4)	U_{33}(O)	0.0050(2)	$F_{\bar{2}20}$	30.04(2)
U_{22}(Fe)	0.00418(10)	U_{23}(O)	0.00097(5)	F_{004}	30.42(2)
U_{11}(Cr)	0.0048(4)	$F_{0\bar{1}1}$	9.84(5)	F_{031}	−0.37(10)
U_{22}(Cr)	0.0034(1)	F_{020}	−17.18(8)	$F_{\bar{1}23}$	−0.52(4)
U_{33}(Cr)	0.0027(1)	$F_{\bar{1}12}$	16.20(1)	F_{024}	9.47(5)
U_{23}(Cr)	0.000011(2)	$F_{\bar{1}21}$	−23.46(5)		

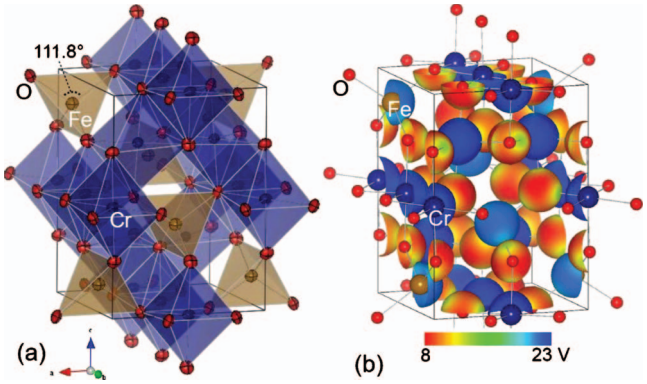

FIG. 3. (Color) (a) ORTEP diagram of refined crystal structure of low-temperature phase of $FeCr_2O_4$. (b) Electron-density isosurface of $0.8e/Å^3$ colored with electrostatic potentials.

Compared with the room-temperature cubic phase, the FeO_4 tetrahedra are found to be compressed in the c direction, and the angle between the neighboring Fe-O bonds is increased from 109.5° to 111.8°. Thus, at the Fe atoms, the $3z^2-r^2$ orbital should be energetically more favorable than the x^2-y^2 orbital in terms of Coulomb repulsion. The refined crystal structure suggests the ferro-type orbital ordering of the $3z^2-r^2$ orbital in the c direction at the Fe atoms.

The electrostatic potential was reconstructed by Fourier synthesis using the refined low-order structure factors as shown in Table I and the other higher-order structure factors up to $g=12.0$ $Å^{-1}$ calculated by using the refined atom positions, atomic displacement parameters, and electron atomic scattering factors for the neutral atoms [independent atom model (IAM)]. The electron-density distribution was obtained from the x-ray structure factor values converted from the structure factor values obtained above using the Mott-Bethe formula, which is a reciprocal-space expression of Poisson's equation. In contour plots of the reconstructed electron density, however, anisotropy around the Fe site was hardly detectable. We can visualize the obtained electrostatic potential and electron density in the form of an electron-density isosurface colored with electrostatic potential, using the software VESTA developed by Momma and Izumi.[30] That is an effective way to visualize the variations in electrostatic potential using electron density as a reference. Figure 3(b) shows such an electron-density isosurface of $0.8e/Å^3$ based on the present result for the entire unit cell. The electrostatic potentials at Fe and Cr sites are higher (blue) and those at the O sites are lower (red), as a natural result of charge transfer from Fe and Cr atoms to O atoms.

To show more details, the Fe tetrahedron of the $4e/Å^3$ isosurface of the room-temperature phase and that of the low-temperature phase are, respectively, shown in Figs. 4(a) and 4(b), with narrower color scales for electrostatic potential. The radii of the spheres of the isosurfaces, at which the probability densities of Fe $3d$ electrons are expected to be higher, are approximately 0.5 Å. In the room-temperature phase, red areas are seen at the positions nearest to the adjacent O sites because of the influence of the O ions with excess electrons. Note that in the low-temperature phase, red areas appear at the top and the bottom of the sphere at Fe

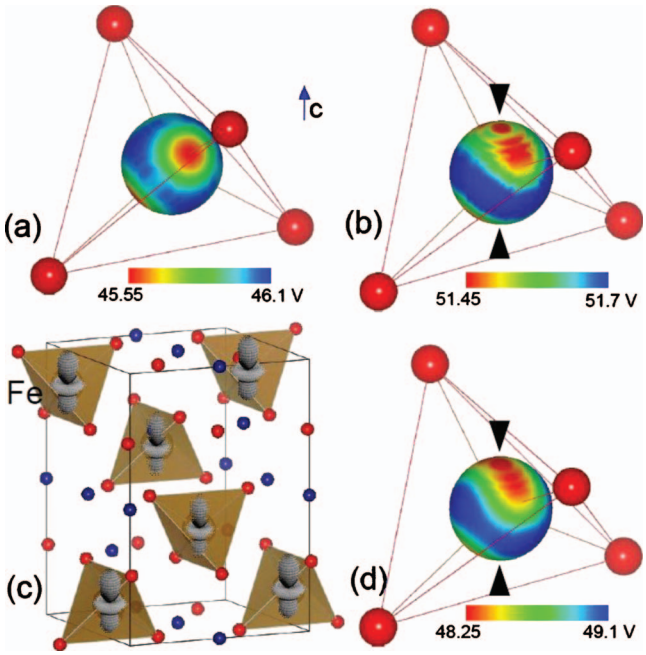

FIG. 4. (Color) (a) $4e/Å^3$ isosurface of FeO_4 tetrahedron of room-temperature cubic phase colored with electrostatic potential and (b) that of low-temperature tetragonal phase. (c) Schematic and (d) $4e/Å^3$ isosurface of hypothetical Fe $3z^2-r^2$ orbital-ordered model.

sites, as well as the areas nearest to the O sites. This can be attributed to the existence of excess electrons due to the $3z^2-r^2$ orbital along the c direction. We conclude that this is direct evidence of the $3z^2-r^2$ orbital ordering in the c direction in the low-temperature phase. No such anisotropy related to orbital ordering was found at the Cr sites, which has no orbital degree of freedom.

Simulations were also conducted using a hypothetical orbital-ordered model. Figure 4(c) schematically shows the hypothetical model of the Fe $3z^2-r^2$ orbitals ordered in the c direction. The electrostatic potential and electron density of the model were obtained from the structure factors calculated using the aspherical scattering factors of the Fe $3z^2-r^2$ orbital[31,32] for the low-order reflections used in the present analysis and the IAM structure factors for the other higher-order reflections. Figure 4(d) shows the isosurface of $4e/Å^3$ colored with the electrostatic potential for the model; Fig. 4(d) agrees well with the experimental result of Fig. 4(b).

It is noted that the red areas in Figs. 4(b) and 4(c) show a few oscillations in the c direction. This is due to the limited number of the low-order structure factors refined in the present analysis. To reduce this effect, additional low-order structure factors must be refined. For this purpose, experimental data highly sensitive to those structure factors, which may be obtained by CBED patterns at different incident directions, are necessary.

In summary, we have applied the CBED nanoscale structure analysis method developed by Tsuda and Tanaka[17,20] to the low-temperature phase of $FeCr_2O_4$. The atom positions,

atomic displacement parameters, and low-order structure factors have been determined, together with the space-group and lattice parameters, using the CBED data alone obtained from single-domain areas, which are a few nanometer in diameter, at 90 K. The electrostatic potential and electron-density distribution have been successively reconstructed from the determined parameters. We have successfully observed the ferro-type ordered state of the Fe $3z^2-r^2$ orbitals in $FeCr_2O_4$ through the obtained electrostatic potential. This method is strongly expected to be applied to the investigation of local fluctuations of orbital-ordered states in various transition-metal oxides. The electrostatic potential analysis using CBED also has great promise for observing electrical polarization in ferroelectric materials.

The authors greatly thank M. Tanaka for valuable discussion and his critical reading, F. Sato for his careful maintenance of our energy-filtering TEM, and M. Terauchi for helpful discussion and support. The present study was partly supported by Grant-in-Aids for Scientific Research (B) (Grants No. 20340070 and No. 19340089) and a Grant-in-Aid for Scientific Research on Priority Areas (Grant No. 19051002) from the Ministry of Education, Culture, Sports, Science and Technology of Japan.

*k˙tsuda@tagen.tohoku.ac.jp

[1] T. Suzuki, M. Katsumura, K. Taniguchi, T. Arima, and T. Katsufuji, Phys. Rev. Lett. **98**, 127203 (2007).
[2] Y. Ito and J. Akimitsu, J. Phys. Soc. Jpn. **40**, 1333 (1976).
[3] J. Akimitsu, H. Ichikawa, N. Eguchi, T. Miyano, M. Nishi, and K. Kakurai, J. Phys. Soc. Jpn. **70**, 3475 (2001).
[4] Y. Murakami, H. Kawada, H. Kawata, M. Tanaka, T. Arima, Y. Moritomo, and Y. Tokura, Phys. Rev. Lett. **80**, 1932 (1998).
[5] I. Zegkinoglou, J. Strempfer, C. S. Nelson, J. P. Hill, J. Chakhalian, C. Bernhard, J. C. Lang, G. Srajer, H. Fukazawa, S. Nakatsuji, Y. Maeno, and B. Keimer, Phys. Rev. Lett. **95**, 136401 (2005).
[6] M. Takata, E. Nishibori, K. Kato, M. Sakata, and Y. Moritomo, J. Phys. Soc. Jpn. **68**, 2190 (1999).
[7] K. Kato, M. Takata, E. Nishibori, M. Sakata, N. Hamada, and Y. Moritomo, J. Phys. Soc. Jpn. **74**, 2137 (2005).
[8] S. B. Wilkins, P. D. Spencer, P. D. Hatton, S. P. Collins, M. D. Roper, D. Prabhakaran, and A. T. Boothroyd, Phys. Rev. Lett. **91**, 167205 (2003).
[9] M. Ito, N. Tuji, F. Itoh, H. Adachi, E. Arakawa, K. Namikawa, H. Nakao, Y. Murakami, Y. Taguchi, and Y. Tokura, J. Phys. Chem. Solids **65**, 1993 (2004).
[10] T. Kiyama, T. Shiraoka, M. Itoh, L. Kano, H. Ichikawa, and J. Akimitsu, Phys. Rev. B **73**, 184422 (2006).
[11] N. Tsuji, M. Ito, H. Sakurai, K. Suzuki, K. Tanaka, K. Kitani, H. Adachi, H. Kawata, A. Koizumi, H. Nakao, Y. Murakami, Y. Taguchi, and Y. Tokura, J. Phys. Soc. Jpn. **77**, 023705 (2008).
[12] J. M. Zuo, J. C. H. Spence, and M. O'Keeffe, Phys. Rev. Lett. **61**, 353 (1988).
[13] C. Deininger, G. Necker, and J. Mayer, Ultramicroscopy **54**, 15 (1994).
[14] M. Saunders, D. M. Bird, N. J. Zaluzec, W. G. Burgess, A. R. Preston, and C. J. Humphreys, Ultramicroscopy **60**, 311 (1995).
[15] M. Saunders, D. M. Bird, O. F. Holbrook, P. A. Midgley, and R. Vincent, Ultramicroscopy **65**, 45 (1996).
[16] J. M. Zuo, M. O'Keeffe, P. Rez, and J. C. H. Spence, Phys. Rev. Lett. **78**, 4777 (1997).
[17] K. Tsuda and M. Tanaka, Acta Crystallogr., Sect. A: Found. Crystallogr. **55**, 939 (1999).
[18] J. M. Zuo, M. Kim, M. O'Keeffe, and J. C. H. Spence, Nature (London) **401**, 49 (1999).
[19] V. A. Streltsov, P. N. H. Nakashima, and A. W. S. Johnson, J. Phys. Chem. Solids **62**, 2109 (2001).
[20] K. Tsuda, Y. Ogata, K. Takagi, T. Hashimoto, and M. Tanaka, Acta Crystallogr., Sect. A: Found. Crystallogr. **58**, 514 (2002).
[21] L. Wu, Y. Zhu, T. Vogt, H. Su, J. W. Davenport, and J. Tafto, Phys. Rev. B **69**, 064501 (2004).
[22] Y. Ogata, K. Tsuda, Y. Akishige, and M. Tanaka, Acta Crystallogr., Sect. A: Found. Crystallogr. **60**, 525 (2004).
[23] Y. Ogata, K. Tsuda, and M. Tanaka, Acta Crystallogr., Sect. A: Found. Crystallogr. **64**, 587 (2008).
[24] J. B. Goodenough, J. Phys. Chem. Solids **25**, 151 (1964).
[25] G. Shirane, D. E. Cox, and S. J. Pickart, J. Appl. Phys. **35**, 954 (1964).
[26] T. Arima, Y. Watanabe, K. Taniguchi, M. Watanabe, and Y. Noda, J. Magn. Magn. Mater. **310**, 807 (2007).
[27] M. Tanaka, *International Tables for Crystallography*, 3rd ed., edited by U. Shumueli (International Union of Crystallography, Springer, Dordrecht, 2008), Vol. B, p. 307.
[28] M. H. Francombe, J. Phys. Chem. Solids **3**, 37 (1957).
[29] M. Ichikawa and K. Hayakawa, J. Phys. Soc. Jpn. **42**, 1957 (1977).
[30] K. Momma and F. Izumi, J. Appl. Crystallogr. **41**, 653 (2008).
[31] R. J. Weiss and A. J. Freeman, J. Phys. Chem. Solids **10**, 147 (1959).
[32] *International Table for X-Ray Crystallography*, edited by J. A. Ibers and W. C. Hamilton (Kynoch Press, Birmingham, 1974), Vol. IV, p. 102.